Published in final edited form as:
J Comput Neurosci. 2015 February ; 38(1): 53–66. doi:10.1007/s10827-014-0526-4.

A Neuron Model of Stochastic Resonance Using Rectangular Pulse Trains

Zachary Danziger[1] and **Warren M Grill**[1,2,3,4]

[1]Duke University, Department of Biomedical Engineering, Durham NC 27708-0281

[2]Duke University, Department of Electrical and Computer Engineering, Durham NC 27708

[3]Duke University, Department of Neurobiology, Durham NC 27710

[4]Duke University, Department of Surgery, Durham NC 27710

Abstract

Stochastic resonance (SR) is the enhanced representation of a weak input signal by the addition of an optimal level of broadband noise to a nonlinear (threshold) system. Since its discovery in the 1980s the domain of input signals shown to be applicable to SR has greatly expanded, from strictly periodic inputs to now nearly any aperiodic forcing function. The perturbations (noise) used to generate SR have also expanded, from white noise to now colored noise or vibrational forcing. This study demonstrates that a new class of perturbations can achieve SR, namely, series of stochastically generated biphasic pulse trains. Using these pulse trains as 'noise' we show that a Hodgkin Huxley model neuron exhibits SR behavior when detecting weak input signals. This result is of particular interest to neuroscience because nearly all artificial neural stimulation is implemented with square current or voltage pulses rather than broadband noise, and this new method may facilitate the translation of the performance gains achievable through SR to neural prosthetics.

1. Introduction

Non-linear threshold systems transmit weak input signals more accurately when exposed to an optimal level of noise, a phenomenon called stochastic resonance (SR) (Gammaitoni et al. 1998). Since neurons are essentially noisy, thresholded, information transfer systems, SR has found multiple applications in neuroscience (McDonnell and Abbott 2009). For example, the nervous system appears to leverage the noise inherent in neural circuits to improve information transfer (Ma et al. 2006; Stein et al. 2005; Faisal et al. 2008), and much current work seeks to explain the mechanisms by which this is accomplished. Another application lies in injecting external noise into the nervous system to create SR, thereby artificially enhancing neural information transfer. Advances on this front have the potential to restore sensitivity and functionality to the damaged or diseased nervous system where, for example, age related or diabetes-induced neuropathy may weaken sensation in the peripheral nervous system (Sumner et al. 2003; Mold et al. 2004). The present study is motivated by

Corresponding Author: Zachary Danziger, Duke University, Department of Biomedical Engineering Campus box 90281, Durham NC, 27710-0281, zd10@duke.edu, Phone: 919-660-5250.

this second aim, and we present an approach to achieve SR that is conducive to artificial stimulation of the nervous system.

Numerous studies have demonstrated improved performance across multiple sensory modalities by artificially introducing an optimal level of noise, but little of this technology has been applied in neural prosthetics outside of the laboratory. For example, SR enhanced performance in photoreceptors (Bahar and Moss 2004), cochlear implants and audition (Jaramillo and Wiesenfeld 1998; Chatterjee and Robert 2001), mechanoreceptors (Collins et al. 1996; Douglass et al. 1993; Manjarrez et al. 2002; Richardson et al. 1998), muscle receptors (Fallon et al. 2004), cardiac regulation (Hidaka et al. 2001), muscle motor units (Kouzaki et al. 2012), finger force production accuracy (Mendez-Balbuena et al. 2012), vibrotactile sensation (Liu et al. 2002), and balance in subjects with neurological deficit (Priplata et al. 2006).

However, there is a disconnect between studies of SR and neural prosthetics: nearly all work on generating and tuning SR employs broadband noise while nearly all neural prosthetics use square pulses to activate the nervous system. In all of the mentioned *in vivo* studies, and in canonical theoretical studies as well (Hanggi et al. 1993; Benzi et al. 1981; Collins et al. 1995; Longtin 1993), SR research was overwhelmingly focused on broadband noise, such as white noise (in fact, this is true of nearly all classical SR studies in the physical sciences, for reviews see (Wellens et al. 2004; Lindner et al. 2004)). This is an obstacle to the implementation of SR in neural prosthetics because by far the most common and studied type of neural stimulation is highly structured pulse trains (Merrill et al. 2005), where a time series of rectangular current or voltage pulses is delivered to the neural tissue. Trains of current pulses are much more suitable than broadband noise for application in neural stimulation because existing devices make pulses easy to implement and the vast literature dealing with electrical stimulation of neural tissue can be brought to bear on the mechanisms and effects of the stimulation. Moreover, this approach is likely to facilitate regulatory approval because a large number of neural stimulation devices that use square stimulation pulses are approved for use in humans (for example peripheral nerve stimulators, spinal cord stimulators and deep brain stimulators), and investigations into electrical stimulation safety focus nearly exclusively on square pulses (Ballestrasse et al. 1985; Agnew et al. 1986; Merrill et al. 2005). Therefore, to advance the development of neural prosthetics that can leverage SR it is necessary to know whether pulse trains can elicit SR behavior in neurons, and how this compares to SR achieved with traditional broadband noise.

The present study demonstrates that charge balanced biphasic pulses delivered with random interpulse intervals and pulse durations elicit classical SR behavior in a computational Hodgkin Huxley model neuron (Hodgkin and Huxley 1952). Moreover, with optimized parameters, the stochastic pulse trains can perform better than broadband noise. These results may facilitate the translation of laboratory studies of SR in the nervous system to neural prosthetics by enabling the use of pulse train perturbations to generate SR, rather than broadband noise.

2. Materials and Methods

2.1. The Model

All analysis was conducted using the canonical Hodgkin Huxley single compartment model neuron (Hodgkin and Huxley 1952). The model equations were numerically integrated in MATLAB R2013a using the Euler method with a fixed step size of 0.025 ms, determined empirically to produce numerically stable results (with the exception of the highest correlation time curve in Fig. 5A which used a step size of 0.01 ms). A single simulation consisted of integrating the model equations for 2075 ms. Model parameters are given in table 1. Model equations and analysis code can be found in Online Resource 1.

The equation describing the neuron's transmembrane voltage is

$$\frac{dV}{\mathrm{dt}} = \left(I_s + I_\delta - \sum\nolimits_r I_r\right)/C_m \quad (1)$$

where V is the transmembrane voltage, I_S is the stimulus current acting as the input signal to the cell, I_δ is a perturbation current applied to achieve stochastic resonance, and I_r is the rth ionic current: sodium, potassium, or leak.

The input signal, I_S, was constructed to mimic a sensory stimulus, such as a series of tactile events, and consisted of a 6 Hz periodic square wave with a duty cycle of 45 % and a linear rise to peak amplitude and fall back to baseline (0 mA) of 18 ms. The peak signal amplitude was constant across each simulation but varied between simulations as indicated for each figure. For data in Fig. 6 the input signals used for each simulation are listed in the figure.

The ionic currents are expressed as

$$\sum\nolimits_r I_r = g_{Na} \cdot m^3 \cdot h \cdot (V - E_{Na}) + g_K \cdot n^4 \cdot (V - E_K) + g_L \cdot (V - E_L)$$

were E_r is the reversal potential of ionic current r, g_r is the maximum membrane conductance of species r, and m, h, and n are the gating variables ranging from zero to one that modify membrane conductance. The gating variable equations are

$$\frac{dm}{\mathrm{dt}} = \frac{(2.5-0.1V)}{(e^{2.5-0.1V}-1)}(1-m) - 4e^{-V/18}m$$
$$\frac{dn}{\mathrm{dt}} = \frac{(0.1-0.01V)}{(e^{1-0.1V}-1)}(1-n) - 0.125e^{-V/80}n$$
$$\frac{dh}{\mathrm{dt}} = 0.07e^{-V/20}(1-h) - \frac{1}{(e^{3-0.1V}+1)}h$$

2.2. Signal Matching Measure

To quantify the degree to which the output of the neuron matched the input signal over each simulation we used a measure related to the “power norm” developed for aperiodic stimuli (Collins et al. 1995):

$$\tilde{C}_1 = \frac{\frac{1}{N}\sum_{k=0}^{k=N} S_k R_k}{RMS[S]\cdot RMS\left[R - \frac{1}{N}\sum_{k=0}^{k=N} R_k\right]} \quad (2)$$

$$RMS[x] = \left(\frac{1}{N}\sum_{k=1}^{k=N} x_k^2\right)^{1/2}$$

Here, S is the input signal to be detected (with mean subtracted), I_S, and R is an indicator variable representing the presence or absence of an action potential at sample k, of which there are N for each simulation. Therefore, this measure is effectively the cross-correlation of S and R at time-lag zero, normalized by the product of their zero-mean RMS amplitudes. This measure of signal matching focuses on the coherence between input and output, and avoids definitions that rely on spectral power ratios, which are incomplete descriptions of a system's ability to represent an aperiodic input signal (Galdi et al. 1998; Inchiosa and Bulsara 1995).

The indicator variable, R, was constructed as a time-series equal in length to the input signal that was zero everywhere except for 2ms windows centered at the time of each action potential (detected by 50 mV thresholding of the membrane potential) that were set to a value of one. R was then used to calculate $\tilde{C_1}$ in equation 2. We transformed the response in this way because it is assumed that the neuron only conveys information through action potentials and that other fluctuations in transmembrane potential do not contribute to signal transmission and should be ignored by the cross-correlation measure. This measure is a slight departure from that presented in Collins et al. 1995 because R in this context is the spike train rather than the firing rate of the neuron.

2.3. Perturbation Parameterization

Biphasic pulse train perturbations, I_δ in equation 1, consisted of rectangular current pulses with a positive leading phase and a negative trailing phase with a combined pulse width of w. Each pulse was separated by an interpulse interval T (see Fig. 3A). Each interpulse interval and pulse width was drawn from uniform distributions. New realizations of the stochastic pulse trains were generated for each simulation. The amplitude of each pulse in the biphasic pulse train was constant during each simulation and calculated as $a = E[A_{rms}]((b_w + a_w)/(b_T + b_w))^{-1/2}$ (see 3.2 in Results), where A_{rms} is the desired RMS amplitude of the pulse train and $E[\cdot]$ is the expected value.

The broadband perturbations were simulated with the Ornstein-Uhlenbeck (OU) process. The discrete OU process stochastic differential equation is

$$dy_t = -r_c y_{t-1}\mathrm{dt} + \sigma\sqrt{2r_c}dW_t \quad dW_t \sim N(0, \mathrm{dt}) \quad (3)$$

where y_t is the process value at time step t, dt is the size of the time step and r_c is the parameter that controls the rate at which the process reverts to the mean set to $r_c = 0.5$ ms^{-1} for all simulations using the OU process unless otherwise indicated (Lee and Kim 1999). The stochastic component, W_t, is the Wiener process, N is the standard normal distribution and σ is the RMS process amplitude. Colored noise, such as the OU process, is often used in

place of pure white noise when studying SR neural systems to provide direct control over the noise correlation time (Yu et al. 2001; Lee and Kim 1999; Longtin 1993).

2.4. Spectral Analysis

Spectral analysis was done using the open source Chronux software (chronux.org) (Mitra and Bokil 2008), implemented with MATLAB R2013a (Mathworks). The double-sided power spectra in Fig. 7 and 8 were calculated using a simulation sampling rate of 40kHz, and are multitaper spectral estimates using 19 tapers.

The noise-like time series with a spectrum matching the stochastic biphasic pulse train was built by randomly generating real and imaginary parts of Fourier coefficients that were scaled by the actual corresponding coefficients from the target biphasic pulse train. The real part of the inverse-Fourier transform was then used to recover the desired noise-like signal in the time domain.

The time series of pulses with a spectrum matching the broadband perturbation was built using a spectral mimicry algorithm that permutes a time series X using the time rank statistics of time series Y to produce a new time series Z such that the spectra of Y and Z are similar (Cohen et al. 1999). Therefore, the mimicry pulse train (Fig. 7, orange) contains precisely the same time points as a realization of a stochastic biphasic pulse train (Fig. 7, black is one example, although it has a different amplitude) only shuffled in time to produce the desired spectrum.

3. Results

3.1. Stochastic Resonance in the Model Neuron

Stochastic resonance (SR) emerges from the interaction of an input signal (what the system attempts to detect), the perturbations (noise that is delivered) and the coherence of the system's output with the input (the system's accuracy or quality of information transmission). We used a single compartment Hodgkin Huxley model neuron as the system and the input signal was an applied current that mimicked a series of stimuli found in typical sensory studies in neurophysiology (Collins et al. 1997; J. Hao and Delmas 2010), and the output of the model was its action potentials.

We first determined how effective the model was at representing signals in the ideal case, when the inputs were strong enough to be detected without SR, and this served as a baseline of comparison for weaker inputs. We applied a zero-noise input signal to the model and varied its amplitude from 5-13 mA. This revealed three distinct response regimes: 1) sub-threshold region where the neuron was silent, 2) threshold level where the neuron fired a constant number of action potentials in response to each stimulus, and 3) supra-threshold levels where the firing rate in response to each stimulus was higher than at the threshold level (Fig. 1). The threshold amplitude was identified as the magnitude of the input signal required to elicit a sustained response throughout each input pulse. At the threshold level the neuron fired 5 action potentials during each 75 ms crest of the input pulse, for an average firing rate of 66.67 Hz.

To quantify the model's accuracy in representing each input signal we used a modified power norm measure, $\tilde{C_1}$, which is effectively a cross-correlation between the model's output and the input signal. Using this measure allowed us to calculate the effect of SR for signals with relevant power in more than one frequency, which is almost always the case for sensory stimuli. The value of $\tilde{C_1}$ produced by the model in response to a threshold-amplitude noiseless input is indicated in fig. 1 as ϕ. Meaning, if $\tilde{C_1} = \phi$. the noise added to generate SR in the presence of a sub-threshold input signal allows the neuron to represent that weak input with the same fidelity as it would represent that same signal at a threshold-level amplitude.

Prior to the signal amplitude crossing the threshold the neuron never fired an action potential, and we define this to be $\tilde{C_1} = 0$. Once the threshold is crossed the neuron begins firing at a frequency that increases with signal amplitude. This frequency determines the number of spikes fired during a given pulse, and thus, $\tilde{C_1}$. When the frequency becomes sufficiently high to fire an additional spike during an input pulse, it appears as a “step” in the $\tilde{C_1}$ measure (Fig. 1). The slight decreasing trend in $\tilde{C_1}$ between these steps is due to the first spike fired by the model in response to an input pulse occurring earlier in the rising phase of that pulse, which is penalized by the normalization procedure in the power norm measure.

It was possible to achieve clear SR behavior in the model neuron using biphasic pulses as “noise”, as well as the traditional broadband noise used in SR studies. To generate SR, we applied an input signal consisting of a series of sub-threshold stimuli (6.5 mA, Fig. 1) to the model and varied the intensity of the additive perturbations (or noise). Fig. 2 shows realizations of three intensities of two types of perturbations: a biphasic pulse train with stochastically determined interpulse intervals and pulse widths and traditional broadband noise. For both perturbation types at low RMS amplitudes the model produced few spikes during a stimulus event, and at high RMS amplitudes the model produced spikes both when the stimulus event was present and when it was not. The model displayed clear SR behavior in response to both perturbation types, exhibiting a single optimal perturbation intensity that produced the maximum $\tilde{C_1}$.

3.2. Optimization of Pulse Trains to Produce SR

The structure of the stochastic biphasic pulse train perturbations used in Fig. 2 was determined by the pulse amplitude, a, and by drawing each interpulse interval, T, and each pulse width, w, independently from separate uniform distributions (Fig. 3A). The time between each pulse varied between b_w and a maximum of b_T. The pulse width varied between a_w and a maximum value of b_w, which ensured that no pulse would start before the previous pulse had ended, thereby eliminating the possibility of pulse summation.

Traditionally, the optimal $\tilde{C_1}$ for SR applications is found by performing a 1-dimensional optimization over the expected perturbation intensity (equivalently, the expected RMS amplitude, $E[A_{rms}]$), which for white noise is a function only of the intensity. However, finding the optimal $\tilde{C_1}$ generated by the stochastic biphasic pulse train perturbation required a 4-dimensional optimization over the parameters a_w, b_w, b_T, and $E[A_{rms}]$. This was not a 6-dimensional optimization because the maximum pulse width was constrained to equal the

minimum interpulse period to avoid overlapping pulses, and after fixing the remaining free parameters the constant pulse amplitude can be calculate as

$$a = E[A_{rms}]((b_w + a_w)/(b_T + b_w))^{-1/2}.$$

Plotting the results of the numerical optimization over the parameter space (excluding the a_w dimension) revealed that $\tilde{C_1}$ is a continuous function of the three parameters, with a number of local maxima (Fig. 3B). The model neuron responses across this parameter space clearly exhibited SR behavior where optimal parameter combinations greatly elevated $\tilde{C_1}$ from base levels of nearly zero. Changes in $\tilde{C_1}$ were quantified over a larger parameter space ($1.5 < b_T < 40$, $0.1 < b_w < 2$, $a_w \in \{0.15,0.25,0.35,0.45\}$) based on typical values used in neural stimulation studies, but for clarity a reduced space was plotted that included the most salient maxima. The $\tilde{C_1}$ measure was least sensitive to the a_w parameter, which was why it was excluded from the parameter space visualization. The average variability (standard deviation) of $\tilde{C_1}$ in response to changes in a_w (0.016) was equivalent to the variability in response to simply repeating the simulations with a new realization of the stochastic pulse train perturbation (0.014), while variability of $\tilde{C_1}$ in response to changes in $E[A_{rms}]$), for example, was approximately 3 times greater (0.045).

It was possible to achieve high $\tilde{C_1}$ using stochastic pulse train perturbations with many different parameter combinations. This resulted in a trade-off between $\tilde{C_1}$ and perturbation amplitude. Short interpulse intervals and long pulse widths achieved $\tilde{C_1}$ values of nearly 0.22, or 0.95ϕ (□ in Fig. 3B), while other parameter combinations resulted in near-optimal $\tilde{C_1}$ values (+ in Fig. 3B) but at less than half of the RMS perturbation amplitude. This trade-off was visualized by plotting all $\tilde{C_1}$ values obtained in the optimization against the RMS amplitude of the pulse train (Fig. 3C), where all parameter combinations that produced at least 85% of the maximum $\tilde{C_1}$ are colored red.

To compare accurately the SR effects of biphasic pulses to that of traditional broadband noise it is important first to explore the possible parameterizations of broadband noise. Colored noise, which is the primary type of perturbations used in SR studies, can be optimized over the expected RMS amplitude, $E[A_{rms}]$, and the noise correlation rate, r_c. An exploration of this parameter space using the Hodgkin-Huxley neuron model (Fig. 4 top) shows that the value of $E[A_{rms}]$ at which the peak $\tilde{C_1}$ occurs decreases as r_c becomes larger, up to approximately r_c=1 ms^{-1}.

This trend of peak $\tilde{C_1}$ at lower $E[A_{rms}]$ as the noise becomes “whiter” has been observed in neurons experimentally (Nozaki et al. 1999) (though this was using $1/f^{\beta}$ noise for increasing β rather than correlation rates), in analytical approximations using the FitzHugh-Nagumo (FN) model (Nozaki et al. 1999), and in double-well potential models (Gammaitoni et al. 1989; Hanggi et al. 1993). These studies also indicate that their SR measures attain higher overall peaks as the noise approaches pure white noise, however, our simulations show very little change in peak $\tilde{C_1}$ across r_c (note the compressed $\tilde{C_1}$ axis in Fig. 4 bottom). This difference is likely due to the dynamics of the Hodgkin-Huxley model used here as opposed to reduced dimensional models that are typically studied. When performing this

optimization using the FN model and the same sub-threshold "trapezoidal" input signal we find the expected increase in overall peak $\tilde{C_1}$ with increasing r_c (see Online Resource 2).

The simulations here also show a rise in $E[A_{rms}]$ needed to reach peak $\tilde{C_1}$ at large noise correlation rates. The range of correlation rates simulated, 0.005-5 ms^{-1}, encompasses the typical rates found in studies using the Hodgkin-Huxley model with colored noise, which are on the order of 0.5 ms^{-1} (Lee and Kim 1999; Yu et al. 2001; Lee et al. 1998) for transmembrane noise, 0.09 and 0.37 ms^{1} for conductance-based noise models (Wenning et al. 2005; Wenning and Obermayer 2003) and 1 ms^{-1} (Gong et al. 2009; Y. H. Hao et al. 2011) or 1.6-3.3 ms^{-1} (Sun and Lu 2014) for network analysis. The increase in $E[A_{rms}]$ needed to reach peak $\tilde{C_1}$ becomes apparent in our simulations only at $r_c > 1$ ms^{-1}. (Our optimization using the FN model did not show this subsequent increase for $r_c > 1$ ms^{-1}.)

To compare the stochastic pulse train to traditional broadband noise perturbations, we fixed the pulse train parameters at the two combinations marked in Fig. 3B, the optimal $\tilde{C_1}$ and the near-optimal but low RMS amplitude combinations, and plotted the resulting 1-dimensional optimization over expected RMS perturbation amplitude (Fig. 5A). Also plotted are broadband noise perturbations with the parameters marked in Fig. 4 and an additional high-correlation rate noise perturbation. All perturbations generated a single peak $\tilde{C_1}$ smoothly approached from each side. The pulse trains were able to achieve higher $\tilde{C_1}$ than broadband noise with low and medium correlation rates; however, these optimum values required greater RMS perturbation amplitudes. At very large correlation rates the shape of the $\tilde{C_1}$ curves began to more closely resemble those generated with biphasic pulses. Examples of simulation segments from each perturbation type are shown in Fig. 5B.

The frequency of the "trapezoidal" input signal (shown in Fig. 5B) was varied to ensure that SR behavior was not confined to a narrow input signal range. $\tilde{C_1}$ vs $E[A_{rms}]$ curves for inputs across numerous periods show that SR persists across many parameterizations of the input signal (Fig. 6A). Threshold amplitudes were determined for each noiseless input signal and the input signals were then applied to the model at 90% of this threshold.

To verify that the SR behavior of the model neuron was not an artifact of the form of the input signal, the simulations were repeated using a number of different inputs. All sub-threshold input signals combined with stochastic biphasic pulse trains produced characteristic SR behavior, indicating the effect is robust to varied signal types. Fig. 6B shows three example $\tilde{C_1}$ curves resulting from a 30Hz sine wave input, a 10Hz cosine input and a random-uniformly distributed series of 2 ms-duration square pulses. Threshold amplitudes were determined for each noiseless input signal and the input signals were then applied to the model at 90% of this threshold. $\tilde{C_1}$ rose to a single peak value for all input signals.

3.3. Spectral Analysis

The stochastic biphasic pulse train is fundamentally different from classical broadband noise perturbations. The (double-sided) power spectral density of the pulse train is not broadband, but rather it consists of a single lobe for which power scales inversely with expected interpulse interval and for which the cutoff is the inverse of the expected pulse width,

$$cutoff = 2/(a_w + b_w) \quad (4)$$

where a_w and b_w are the minimum and maximum allowable pulse width, respectively. The difference is clearly visible where the stochastic biphasic pulse train (red) produces a lobe of spectral power (cutoff 1.31 kHz) while the broadband noise (blue) simply falls off with frequency (Fig. 7).

The spectral content of the perturbations appears to be more relevant to the character of the $\tilde{C_1}$ response than the time-domain content. The previously described broadband (blue) and stochastic biphasic pulse perturbations (red) were used to generate $\tilde{C_1}$ curves across perturbation amplitudes (using the sub-threshold input signal described in Fig. 1), and they exhibited markedly different SR behavior, with peak $\tilde{C_1}$ separated by 8 mA RMS amplitude. Next we generated a perturbation that was similar to broadband noise in the time domain, but which had a power spectrum that matched the stochastic biphasic pulse train (black). Fig. 7 shows that the $\tilde{C_1}$ curve for this perturbation was clearly more similar to the stochastic biphasic pulse $\tilde{C_1}$ curve than to the broadband noise curve. Further, we generated a perturbation consisting of only stochastic square pulses (although not strictly biphasic or charged balanced), which had a spectrum that matched the broadband noise (orange). The $\tilde{C_1}$ curve with this pulse train was clearly more similar to the broadband noise curve. These results suggest that the distribution of spectral power in the perturbations is the primary factor driving the shape of SR responses. Moreover, these results show, in principle, that a time series using only square pulses can be generated that will create many different SR peak heights, locations and widths. This is promising because nearly all neural stimulation devices operate with square pulses, and thus would be capable of eliciting and tuning SR behavior in the excitable tissue.

The spectra in Fig. 7 also show that using stochastic biphasic pulses as “noise” is a clear departure from work that generates SR in neuron populations using pulses as a stand-in for distributed synaptic events (Stacey and Durand 2000; Teramae et al. 2012; Mino and Durand 2010; Droste et al. 2013) because such perturbations are deliberately constructed to have a white spectrum of event frequencies, and therefore act as broadband noise. These studies also focus on SR as an internal phenomenon of neural networks, rather than as an external artificial perturbation, and as such conceptualize the pulses as delta functions integrated over the synapses of the network elements.

The effectiveness of SR in bistable systems with external forcing can be modulated by manipulating the correlation time of the broadband noise added to the system (Casado 1997; Hanggi et al. 1993). Such studies typically model the noise as an Ornstein-Uhlenbeck (OU) process where the correlation time (or the inverse of which, the correlation rate, r_c) is the degree of correlation between successive values of the noise process. In fact, the ideal correlation time of broadband noise to produce SR should be on the order of the fast time scale of the neuron, meaning its action potential dynamics. Increasing the correlation time beyond that regime will require an increase in noise intensity to achieve the same signal-to-noise ratio because more of the noise power will be located in the high frequency range that is effectively filtered out by the neuron dynamics (Lindner et al. 2004). This means that as

the correlation time approaches zero (white noise) more spectral power will be located at frequencies beyond the neuron's fast dynamics and will attenuate the effects of SR. For stochastic pulse train perturbations the frequency limit of spectral power concentration is determined by the lobe cutoff frequency (equation 4 and Fig. 7). The lobe cutoff frequency is, therefore, the stochastic pulse train analogue to the broadband noise correlation time.

Fig. 8 shows that as the lobe cutoff frequency increases more power is required to achieve a desired $\tilde{C_1}$; each spectrum corresponds to a stochastic pulse train that achieved $\tilde{C_1}$ of 0.16, and for larger cutoffs larger RMS amplitudes were needed. The inset shows spectra from biphasic pulse trains with the same cutoffs as the main panel but with equal RMS amplitude (and therefore unequal resulting $\tilde{C_1}$). In these spectra more power is distributed at higher frequencies, which are filtered out by the membrane dynamics. For the pulse trains (resulting in the spectra in the inset) to achieve equivalent $\tilde{C_1}$ the RMS amplitude of the stochastic pulse train must be scaled to the point where there exists appropriate power in the critical low frequency range, as indicated by the main panel where the slopes of the spectra at low frequencies are similar. This is consistent with previous results showing that as broadband noise correlation time decreases, and more spectral power is located at higher frequencies, that SR becomes more difficult to achieve (Lindner et al. 2004).

4. Discussion

Laboratory studies over many years and spanning many sensory modalities have shown that artificial SR can enhance or restore human function, but these results have not been translated to assistive devices. In part, this is due to the broadband noise source that is universally used to generate SR, as opposed to trains of rectangular pulses common to nearly all neural stimulation studies and neural prosthetics (Merrill et al. 2005). This study demonstrates (using a Hodgkin Huxley model neuron) that it is possible to induce and tune SR using classic square pulse trains. This advance is important as it initiates a straightforward path between laboratory results and potential translational neuroscience technology that leverages SR. This approach may encourage the development of neural prosthetics that enhance the body's native sensory systems, perhaps to offset neuropathy or other diseases (Hanggi 2002; McDonnell and Abbott 2009), a prospect that has been motivating work in neuroscience SR for at least two decades.

We showed that the spectral content of the noise appears to be the main determining factor in the character of SR behavior, rather than the time domain dynamics, even when those dynamics differ significantly between square pulses and random processes (Fig. 7). It appears possible, therefore, to manipulate the perturbation (noise) spectrum to control the peak SNR location along the perturbation intensity dimension, as well as the width of the peak. Moreover, these manipulations can be made using only square pulse waveforms, meaning they could be implemented using existing technology. The results also showed that the correlation time of broadband noise, a feature that has been investigated in SR studies, has a stochastic biphasic pulse train analogue in the lobe cutoff frequency, suggesting that the membrane filtering mechanisms that shape SR when using broadband noise play a similar role when SR is generated with the biphasic pulse trains.

The optimization of $\tilde{C_1}$ over the stochastic pulse train parameters revealed tradeoffs between high $\tilde{C_1}$ and low perturbation amplitude (Figs. 2A, 3B and 3C). At short interpulse intervals and long pulse widths, $\tilde{C_1}$ approached 0.95ϕ, or 95% of the fidelity achieved when representing noiseless threshold-level inputs. These parameters generated high duty cycle pulse trains that, in the limit, mimic a dc perturbation. Of course, a true dc offset would also achieve "stochastic" resonance in the model; but in practice dc current may corrode the stimulating electrodes and result in tissue damage. Other parameter combinations resulted in high, near-optimal $\tilde{C_1}$ values ('+' in Fig. 3B), but achieved this performance at less than half of the RMS perturbation amplitude. To obtain the highest possible $\tilde{C_1}$ or near-optimal $\tilde{C_1}$ at greatly reduced RMS amplitude is a tradeoff whose resolution will be application specific.

It is important to estimate the relevance of a given $\tilde{C_1}$ value in terms of behavior or performance to put the results in context and to determine an appropriate compromise between RMS perturbation amplitude and $\tilde{C_1}$. For example, Fig. 5A shows a high amplitude perturbation parameterization with a maximum $\tilde{C_1}$ of roughly 0.22 (orange) and a low amplitude perturbation parameterization with a maximum $\tilde{C_1}$ of roughly 0.20 (green), but the functional importance of the 0.02 reduction in $\tilde{C_1}$ is not clear. An accurate answer likely requires an understanding of the way information is encoded in action potentials, how the sensory neuron in question interacts with local circuitry to process the information, and perhaps even how the sensory information is used by executive centers for decision making.

We turned to the results of two psychometric studies to estimate the behavioral significance of changes in $\tilde{C_1}$. The first study showed that the distribution of average neural firing rates during a stimulus presentation has a receiver operator characteristic that matches the psychometric curve of a monkey performing a tactile discrimination task, suggesting that average firing rates of sensory-related neurons contribute to (or at least correlate with) sensory discrimination at a behavioral level (Hernandez et al. 2000). Moreover, these firing rates changed linearly with stimulus intensity. The second study showed that classical SR enhances people's ability to detect accurately sub-threshold tactile impulses (Collins et al. 1997) of roughly the same shape as the "trapezoidal" pulses presented to the model neuron in the current study. These psychometric results indicate that tactile discrimination acuity can be enhanced by SR, and that the average firing rate of our model neuron can be used as a proxy for sensory discrimination. Therefore, the sub-threshold input signal to the model neuron can be viewed as a series of sub-threshold tactile perturbations, and the average firing rate of the neuron maps to a point on a psychometric curve indicating the expected classification of a tactile event. The input signal can then be binned into segments where it is either maximum or zero, and the average firing rate during those bins determines the neuron's classification: either an event was present or no event was present. We assume that the average firing rate during a threshold level stimulus ($\tilde{C_1} = \phi$, 67 Hz, Fig. 1) or higher corresponds to always classifying a bin as having an event, a firing rate of zero corresponds to never classifying the bin as having an event, and the probability of classifying a bin as having an event between the extremes is the firing rate normalized by 67 Hz.

The simple linear relation between average firing rate and bin classification yields an estimate of the impact that changes in $\tilde{C_1}$ have on a behavioral outcome, and shows that a reduction of 0.02 $\tilde{C_1}$ from its peak results in a 5.3% loss in discrimination accuracy (Fig.

9A). In this figure the average percent correct curve is superimposed on the corresponding $\tilde{C_1}$ for a simulation where a stochastic biphasic pulse train was added to the sub-threshold input signal, and shows, as expected, that the peak $\tilde{C_1}$ corresponds to the best performance. This 5.3% loss in accuracy represents a substantial amount, 15.6% of the total range from the maximum of 83.8% correct to chance levels of 50%. Of course, because the performance and $\tilde{C_1}$ curves are not linear, a reduction in $\tilde{C_1}$ will result in different performance losses depending on the location in the curve. The maximum performance value of approximately 84% correct classifications is in rough agreement with previous sub-threshold tactile discrimination behavioral studies that report between 70 to 76% correct at peak performance, depending on subject (Collins et al. 1997). The separation between the average firing rate during bins with (red) and without (black) a stimulus present is the determining factor in the shape of both the $\tilde{C_1}$ and performance curves (Fig. 9B). At low perturbation amplitudes the neuron rarely fires, and classifies every bin as having no event, attaining 50% accuracy because half the bins actually have no event. As the distance between the two curves grows it reaches a point of maximum distinguishability, corresponding to peak performance (8.6 mA RMS amplitude), after which point false positives begin occurring frequently because the firing rate increases during bins without events. This analysis provides an approximation of how the gain of $\tilde{C_1}$ due to SR translates into a measurable performance variable.

The broad potential applicability of SR in biology has motivated numerous studies into how systems can exploit SR, what signals are best suited to benefit from SR and even how the noise used to generate SR can be tuned to boost its effects (McDonnell and Abbott 2009). In addition to optimizing the noise color for SR (Hanggi et al. 1993), work has been done to show how incorporating deterministic perturbations with noise can supplement SR. Extended alternating sub-threshold DC offsets have been shown effectively to reduce the barrier for a system to become excited, or switch to a new stable state, thereby enhancing SR (Mason et al. 2000). High frequency (with respect to the signal to be detected) sinusoids have also been combined with noise to produce a reduction in the noise intensity that otherwise would have been needed to reach the optimal SNR (Ullner et al. 2003). The present study builds on these ideas and demonstrates that perturbations comprised only of square pulses, which are ideally suited for bioengineering applications, can also be used to generate and tune SR. There is no need for extended offsets that can damage neurons and electrodes, and the flexibility of square pulses readily permits asymmetric charge-balanced pulse designs, bursts of pulses, pulses at irregular intervals and other stimulation strategies that are often used in neuroscience and bioengineering. This result promotes new ways to examine how the nervous system uses SR for signal detection and processing, and to exploit SR to restore function to the damaged or diseased nervous system.

Supplementary Material

Refer to Web version on PubMed Central for supplementary material.

Acknowledgments

This work was supported in part by NIH grants R01 NS050514 and T32 NS051156.

References

Agnew WF, Yuen TGH, Mccreery DB, Bullara LA. Histopathologic Evaluation of Prolonged Intracortical Electrical-Stimulation. Exp Neurol. 1986; 92(1):162–185.10.1016/0014-4886(86)90132-9 [PubMed: 3956647]

Bahar S, Moss F. Stochastic resonance and synchronization in the crayfish caudal photoreceptor. Math Biosci. 2004; 188:81–97. Research Support, Non-U.S. Gov't Research Support, U.S. Gov't, Non-P.H.S. Research Support, U.S. Gov't, P.H.S. 10.1016/j.mbs.2003.09.004 [PubMed: 14766095]

Ballestrasse CL, Ruggeri RT, Beck TR. Calculations of the Ph Changes Produced in Body Tissue by a Spherical Stimulation Electrode. Ann Biomed Eng. 1985; 13(5):405–424.10.1007/Bf02407769 [PubMed: 4073626]

Benzi R, Sutera A, Vulpiani A. The Mechanism of Stochastic Resonance. Journal of Physics a-Mathematical and General. 1981; 14(11):L453–L457.10.1088/0305-4470/14/11/006

Casado JM. Noise-induced coherence in an excitable system. Physics Letters A. 1997; 235(5):489–492.10.1016/S0375-9601(97)00648-8

Chatterjee M, Robert ME. Noise enhances modulation sensitivity in cochlear implant listeners: Stochastic resonance in a prosthetic sensory system? Jaro. 2001; 2(2):159–171.10.1007/s101620010079 [PubMed: 11550525]

Cohen JE, Newman CM, Cohen AE, Petchey OL, Gonzalez A. Spectral mimicry: A method of synthesizing matching time series with different Fourier spectra. Circuits Systems and Signal Processing. 1999; 18(4):431–442.10.1007/Bf01200792

Collins JJ, Chow CC, Capela AC, Imhoff TT. Noise-Enhanced Information Transmission in Rat SA1 Cutaneous Mechanoreceptors via Aperiodic Stochastic Resonance. Phys Rev E Stat Phys Plasmas Fluids Relat Interdiscip Topics. 1996; 54(5):5575–5584. [PubMed: 9965744]

Collins JJ, Chow CC, Imhoff TT. Aperiodic stochastic resonance in excitable systems. Phys Rev E Stat Phys Plasmas Fluids Relat Interdiscip Topics. 1995; 52(4):R3321–R3324. [PubMed: 9963950]

Collins JJ, Imhoff TT, Grigg P. Noise-mediated enhancements and decrements in human tactile sensation. Physical Review E. 1997; 56(1):923–926.

Douglass JK, Wilkens L, Pantazelou E, Moss F. Noise enhancement of information transfer in crayfish mechanoreceptors by stochastic resonance. Nature. 1993; 365(6444):337–340. In Vitro Research Support, U.S. Gov't, Non-P.H.S. 10.1038/365337a0 [PubMed: 8377824]

Droste F, Schwalger T, Lindner B. Interplay of two signals in a neuron with heterogeneous synaptic short-term plasticity. Frontiers in Computational Neuroscience. 2013; 7 doi:Unsp 86 Doi 10.3389/Fncom.2013.00086.

Faisal AA, Selen LPJ, Wolpert DM. Noise in the nervous system. Nature Reviews Neuroscience. 2008; 9(4):292–303.10.1038/Nrn2258

Fallon JB, Carr RW, Morgan DL. Stochastic resonance in muscle receptors. J Neurophysiol. 2004; 91(6):2429–2436. Research Support, Non-U.S. Gov't. 10.1152/jn.00928.2003 [PubMed: 14736865]

Galdi V, Pierro V, Pinto IM. Evaluation of stochastic-resonance-based detectors of weak harmonic signals in additive white Gaussian noise. Physical Review E. 1998; 57(6):6470–6479.10.1103/PhysRevE.57.6470

Gammaitoni L, Hanggi P, Jung P, Marchesoni F. Stochastic resonance. Reviews of Modern Physics. 1998; 70(1):223–287.10.1103/RevModPhys.70.223

Gammaitoni L, Menichella-Saetta E, Marchesoni F, Presilla C. Periodically time-modulated bistable systems: Stochastic resonance. Physical Review A. 1989; 40(4):2114–2119.10.1103/PhysRevA.40.2114 [PubMed: 9902370]

Gong YB, Hao YH, Xie YH, Ma XG, Yang CL. Non-Gaussian noise optimized spiking activity of Hodgkin-Huxley neurons on random complex networks. Biophysical Chemistry. 2009; 144(1-2):88–93.10.1016/j.bpc.2009.07.001 [PubMed: 19631448]

Hanggi P. Stochastic resonance in biology. How noise can enhance detection of weak signals and help improve biological information processing. Chemphyschem. 2002; 3(3):285–290. Research Support, U.S. Gov't, Non-P.H.S. 10.1002/1439-7641(20020315)3:3<285: :AID-CPHC285>3.0.CO;2-A [PubMed: 12503175]

Hanggi P, Jung P, Zerbe C, Moss F. Can Colored Noise Improve Stochastic Resonance. Journal of Statistical Physics. 1993; 70(1-2):25–47.10.1007/Bf01053952

Hao J, Delmas P. Multiple desensitization mechanisms of mechanotransducer channels shape firing of mechanosensory neurons. J Neurosci. 2010; 30(40):13384–13395. Research Support, Non-U.S. Gov't. 10.1523/JNEUROSCI.2926-10.2010 [PubMed: 20926665]

Hao YH, Gong YB, Wang L, Ma XG, Yang CL. Single or multiple synchronization transitions in scale-free neuronal networks with electrical or chemical coupling. Chaos Solitons & Fractals. 2011; 44(4-5):260–268.10.1016/j.chaos.2011.02.005

Hernandez A, Zainos A, Romo R. Neuronal correlates of sensory discrimination in the somatosensory cortex. Proceedings of the National Academy of Sciences of the United States of America. 2000; 97(11):6191–6196.10.1073/pnas.120018597 [PubMed: 10811922]

Hidaka I, Ando SI, Shigematsu H, Sakai K, Setoguchi S, Seto T, et al. Noise-Enhanced Heart Rate and Sympathetic Nerve Responses to Oscillatory Lower Body Negative Pressure in Humans. J Neurophysiol. 2001; 86(2):559–564. [PubMed: 11495931]

Hodgkin AL, Huxley AF. A Quantitative Description of Membrane Current and Its Application to Conduction and Excitation in Nerve. Journal of Physiology-London. 1952; 117(4):500–544.

Inchiosa ME, Bulsara AR. Nonlinear Dynamic Elements with Noisy Sinusoidal Forcing -Enhancing Response Via Nonlinear Coupling. Physical Review E. 1995; 52(1):327–339.10.1103/PhysRevE.52.327

Jaramillo F, Wiesenfeld K. Mechanoelectrical transduction assisted by Brownian motion: a role for noise in the auditory system. Nature Neuroscience. 1998; 1(5):384–388.10.1038/1597

Kouzaki M, Kimura T, Yoshitake Y, Hayashi T, Moritani T. Subthreshold electrical stimulation reduces motor unit discharge variability and decreases the force fluctuations of plantar flexion. Neurosci Lett. 201210.1016/j.neulet.2012.02.020

Lee SG, Kim S. Parameter dependence of stochastic resonance in the stochastic Hodgkin-Huxley neuron. Physical Review E. 1999; 60(1):826–830.

Lee SG, Neiman A, Kim S. Coherence resonance in a Hodgkin-Huxley neuron. Physical Review E. 1998; 57(3):3292–3297.10.1103/PhysRevE.57.3292

Lindner B, Garcia-Ojalvo J, Neiman A, Schimansky-Geier L. Effects of noise in excitable systems. Physics Reports-Review Section of Physics Letters. 2004; 392(6):321–424.10.1016/j.physrep.2003.10.015

Liu W, Lipsitz LA, Montero-Odasso M, Bean J, Kerrigan DC, Collins JJ. Noise-enhanced vibrotactile sensitivity in older adults, patients with stroke, and patients with diabetic neuropathy. Arch Phys Med Rehabil. 2002; 83(2):171–176.10.1053/apmr.2002.28025 [PubMed: 11833019]

Longtin A. Stochastic Resonance in Neuron Models. Journal of Statistical Physics. 1993; 70(1-2):309–327.10.1007/Bf01053970

Ma WJ, Beck JM, Latham PE, Pouget A. Bayesian inference with probabilistic population codes. Nature Neuroscience. 2006; 9(11):1432–1438.10.1038/Nn1790

Manjarrez E, Diez-Martinez O, Mendez I, Flores A. Stochastic resonance in human electroencephalographic activity elicited by mechanical tactile stimuli. Neurosci Lett. 2002; 324(3):213–216. [PubMed: 12009526]

Mason J, Lindner JF, Neff J, Ditto WL, Bulsara AR, Spano ML. Pulse-enhanced stochastic resonance. Physics Letters A. 2000; 277(1):13–17.10.1016/S0375-9601(00)00665-4

McDonnell MD, Abbott D. What Is Stochastic Resonance? Definitions, Misconceptions, Debates, and Its Relevance to Biology. PLoS Comput Biol. 2009; 5(5) doi:ARTN e1000348 DOI 10.1371/journal.pcbi.1000348.

Mendez-Balbuena I, Manjarrez E, Schulte-Monting J, Huethe F, Tapia JA, Hepp-Reymond MC, et al. Improved Sensorimotor Performance via Stochastic Resonance. Journal of Neuroscience. 2012; 32(36):12612–12618.10.1523/Jneurosci.0680-12.2012 [PubMed: 22956850]

Merrill DR, Bikson M, Jefferys JGR. Electrical stimulation of excitable tissue: design of efficacious and safe protocols. Journal of Neuroscience Methods. 2005; 141(2):171–198.10.1016/j.jneumeth.2004.10.020 [PubMed: 15661300]

Mino H, Durand DM. Enhancement of information transmission of sub-threshold signals applied to distal positions of dendritic trees in hippocampal CA1 neuron models with stochastic resonance. Biol Cybern. 2010; 103(3):227–236.10.1007/s00422-010-0395-5 [PubMed: 20552219]

Mitra, P.; Bokil, H. Observed brain dynamics. Oxford; New York: Oxford University Press; 2008.

Mold JW, Vesely SK, Keyl BA, Schenk JB, Roberts M. The prevalence, predictors, and consequences of peripheral sensory neuropathy in older patients. J Am Board Fam Pract. 2004; 17(5):309–318. Review. [PubMed: 15355943]

Nozaki D, Mar DJ, Grigg P, Collins JJ. Effects of colored noise on stochastic resonance in sensory neurons. Physical Review Letters. 1999; 82(11):2402–2405.10.1103/PhysRevLett.82.2402

Priplata AA, Patritti BL, Niemi JB, Hughes R, Gravelle DC, Lipsitz LA, et al. Noise-enhanced balance control in patients with diabetes and patients with stroke. Ann Neurol. 2006; 59(1):4–12. Research Support, N.I.H., Extramural Research Support, Non-U.S. Gov't. 10.1002/ana.20670 [PubMed: 16287079]

Richardson KA, Imhoff TT, Grigg P, Collins JJ. Using electrical noise to enhance the ability of humans to detect subthreshold mechanical cutaneous stimuli. Chaos. 1998; 8(3):599–603.10.1063/1.166341 [PubMed: 12779763]

Stacey WC, Durand DM. Stochastic resonance improves signal detection in hippocampal CA1 neurons. J Neurophysiol. 2000; 83(3):1394–1402. [PubMed: 10712466]

Stein RB, Gossen ER, Jones KE. Neuronal variability: Noise or part of the signal? Nature Reviews Neuroscience. 2005; 6(5):389–397.10.1038/Nrn1668

Sumner CJ, Sheth S, Griffin JW, Cornblath DR, Polydefkis M. The spectrum of neuropathy in diabetes and impaired glucose tolerance. Neurology. 2003; 60(1):108–111. Clinical Trial Comparative Study Research Support, Non-U.S. Gov't Research Support, U.S. Gov't, P.H.S. [PubMed: 12525727]

Sun XJ, Lu QS. Non-Gaussian Colored Noise Optimized Spatial Coherence of a Hodgkin-Huxley Neuronal Network. Chinese Physics Letters. 2014; 31(2) doi:Artn 020502 Doi 10.1088/0256-307x/31/2/020502.

Teramae J, Tsubo Y, Fukai T. Optimal spike-based communication in excitable networks with strong-sparse and weak-dense links. Scientific Reports. 2012; 2 doi:Artn 485 Doi 10.1038/Srep00485.

Ullner E, Zaikin A, Garcia-Ojalvo J, Bascones R, Kurths J. Vibrational resonance and vibrational propagation in excitable systems. Physics Letters A. 2003; 312(5-6):348–354.10.1016/S0375-9601(03)00681-9

Wellens T, Shatokhin V, Buchleitner A. Stochastic resonance. Reports on Progress in Physics. 2004; 67(1):45–105. doi:Pii S0034-4885(04)31707-0 Doi 10.1088/0034-4885/67/1/R02.

Wenning G, Hoch T, Obermayer K. Detection of pulses in a colored noise setting. Physical Review E. 2005; 71(2) doi:Artn 021902 Doi 10.1103/Physreve.71.021902.

Wenning G, Obermayer K. Activity driven adaptive stochastic resonance. Physical Review Letters. 2003; 90(12) doi:Artn 120602 Doi 10.1103/Physrevlett.90.120602.

Yu YG, Wang W, Wang JF, Liu F. Resonance-enhanced signal detection and transduction in the Hodgkin-Huxley neuronal systems. Physical Review E. 2001; 63(2)

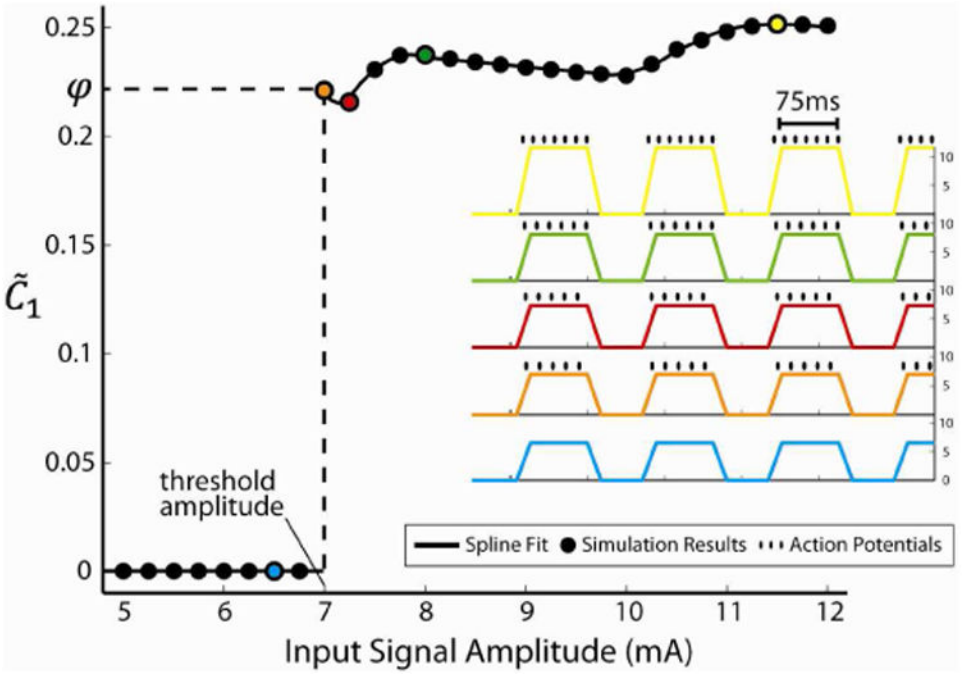

Fig. 1.

The model neuron's ability to represent a noiseless input signal as a function of signal amplitude. Sub-threshold magnitude signals (<7 mA) that elicited no response from the model are considered weak inputs and can benefit from noise perturbations that produce SR. Once threshold is reached, the model fired a constant number of times in response to each stimulus in the input signal. The inset shows the input signal (colored traces), which is a series of stimulus events, and the model neuron's response (raster above each trace) at key signal magnitudes. The model's response is quantified using a version of the power norm measure ($\tilde{C_1}$).

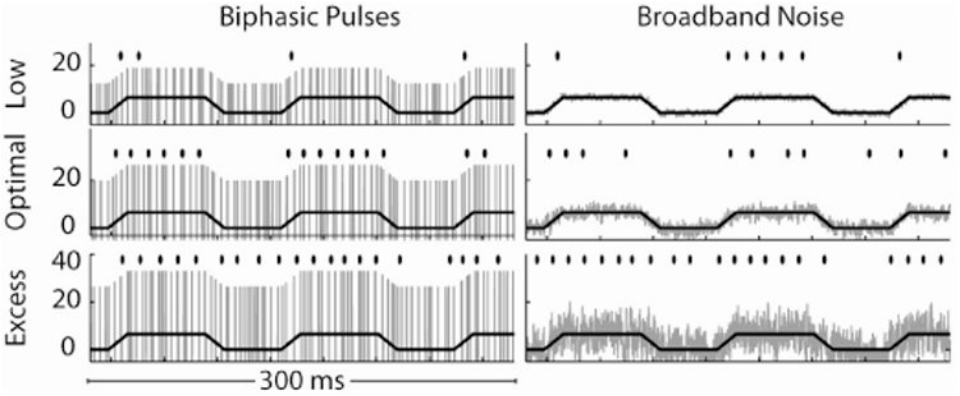

Fig. 2.

Simulation segments illustrating SR in the model neuron in response to stochastic biphasic pulse train and broadband noise perturbations. Realizations of perturbations (gray traces) added to a sub-threshold input signal (black traces) and the model's response (raster above each trace). Each trace is a segment taken from longer simulations (2075 ms) with $\tilde{C_1}$ approximately matched between the two perturbation types. $\tilde{C_1}$ for biphasic pulses are 0.14, 0.20, 0.07 and broadband noise are 0.08, 0.15, 0.06 for low, optimal and excess levels respectively. The RMS amplitudes of the perturbations are 4.62, 8.24, and 11.86 mA for the biphasic pulses and 0.6, 1.5, and 4.5 mA for the broadband noise. The parameters of the biphasic pulse trains correspond to the open circles in Fig. 3B. The broadband noise correlation rate is 0.5 ms^{-1}.

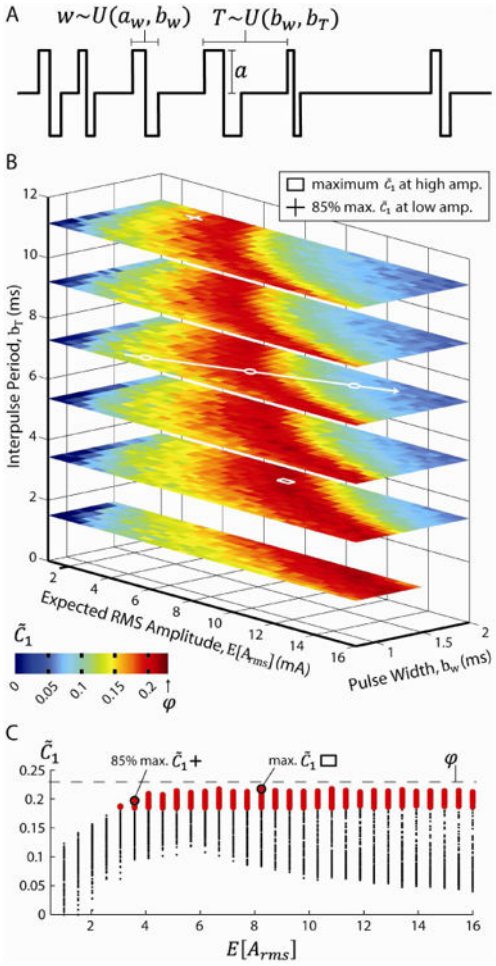

Fig. 3.

Stochastic biphasic pulse train perturbations generated SR in the model neuron. (A) The biphasic pulse train used as the perturbation. Each pulse width, *w*, and period, *T*, was drawn independently from uniform distributions, $X \sim U(X_{min}, X_{max})$. The pulse amplitude, *a*, was constant during each simulation. (B) $\tilde{C_1}$ across the pulse train parameter space. Each cell is the average $\tilde{C_1}$ of eight 2075 ms simulations in response to sub-threshold input signals (Fig. 1). The input signals were identical across all simulations, though realizations of the stochastic pulse train perturbations varied. The a_w parameter was fixed at 0.15. The open circles indicate the parameter combinations used to create the example traces using biphasic pulse train perturbations in Fig. 2. (C) Scatter-plot of all $\tilde{C_1}$ values in (B) versus expected RMS perturbation amplitude. Red points are >85% of the maximum $\tilde{C_1}$.

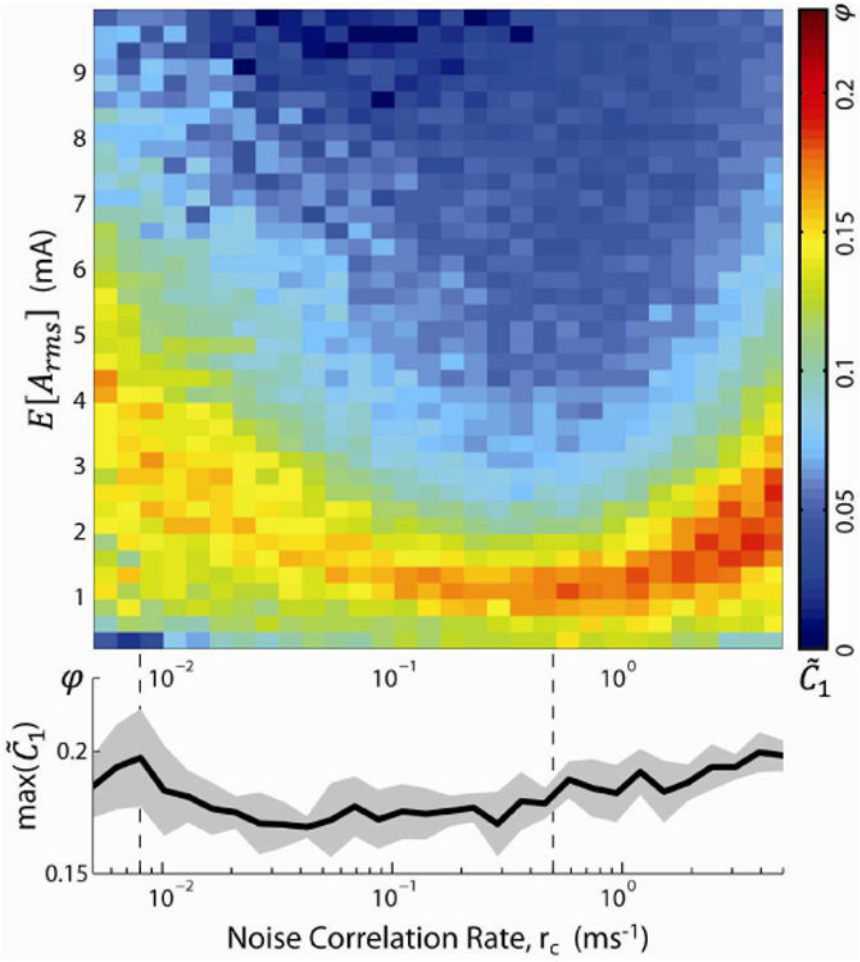

Fig. 4.

Parameter optimization of $\tilde{C_1}$ for broadband noise. The top panel shows $\tilde{C_1}$ as a function of the noise correlation rate, r_c and expected RMS amplitude. Each cell is the average $\tilde{C_1}$ of eight 2075 ms simulations in response to sub-threshold input signals (Fig. 1). The bottom panel shows the average maximum $\tilde{C_1}$ across r_c (black line) and one standard deviation about the mean (gray patch). Vertical dashed lines denote correlation rates used in Fig. 5.

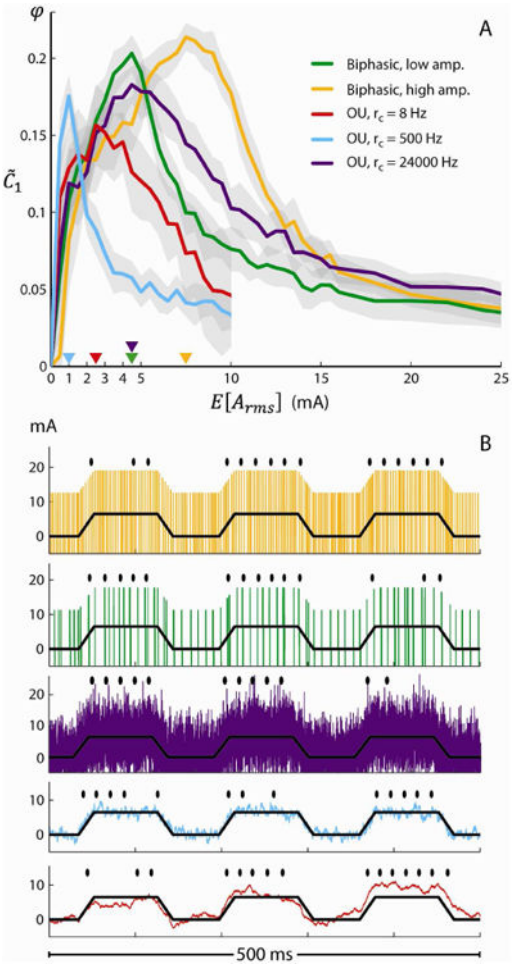

Fig. 5.

A broad range of perturbations generated SR in a model neuron. (A) $\tilde{C_1}$ with traditional broadband noise as a function of expected perturbation amplitude compared with optimal and near-optimal but low RMS amplitude stochastic pulse trains. Parameters for the biphasic pulses are marked in Fig. 3B as "+" and "□" and for broadband noise in Fig. 4 as dashed vertical lines for r_c of 8 and 500 Hz. Lines are the average, and gray regions indicate one standard deviation (n=20 simulations). (B) Realizations of the perturbation types, biphasic pulses at high RMS amplitude, at low RMS amplitude, OU noise with high, medium and low correlation rates, from top to bottom. The input signals are black, the perturbations are colored, and the rasters mark the model's action potential responses. The examples are taken at peak $\tilde{C_1}$ for each type and the corresponding RMS amplitude of each realization is marked by triangles in panel A.

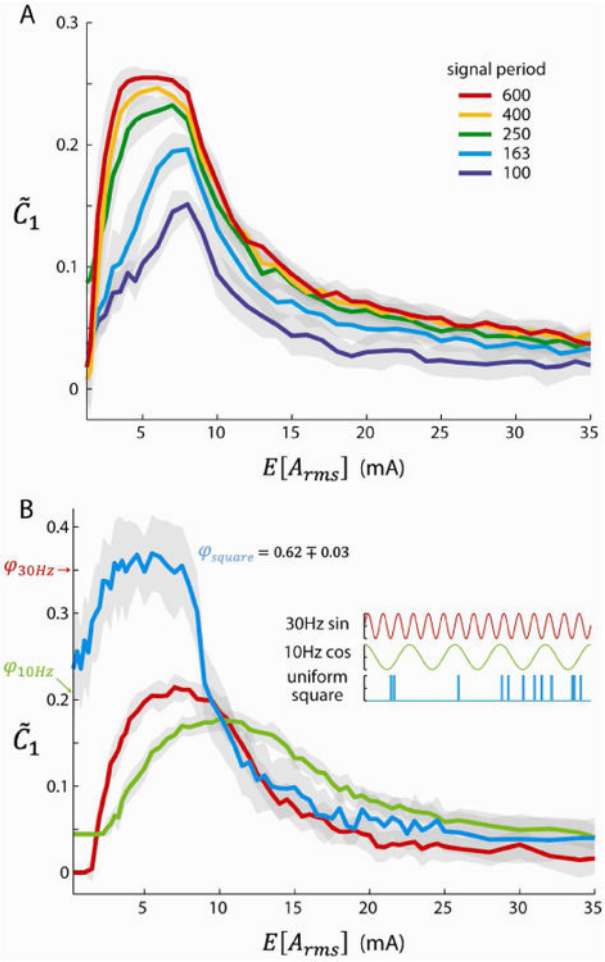

Fig. 6.

The model exhibited SR behavior in response to varied input signals. (A) $\tilde{C_1}$ curves for the "trapezoidal" input signal shown in Fig. 5B at various interpulse periods, showing SR across input signal frequencies when stochastic biphasic pulse perturbations are applied. (B) The model exhibited SR behavior in response to different types of input signals. $\tilde{C_1}$ is plotted in response to subthreshold inputs of either a 30 Hz sine wave, a 10 Hz cosine wave or a random series of square pulses as the input signal (inset). The parameters of the perturbations in panels A and B were stochastic biphasic pulses and followed the white line through parameter space indicated in Fig. 3B. Each trace is the mean $\tilde{C_1}$ over n=20 repetitions and gray bands are one standard deviation. Each input signal was scaled to 90% of its respective threshold RMS amplitude.

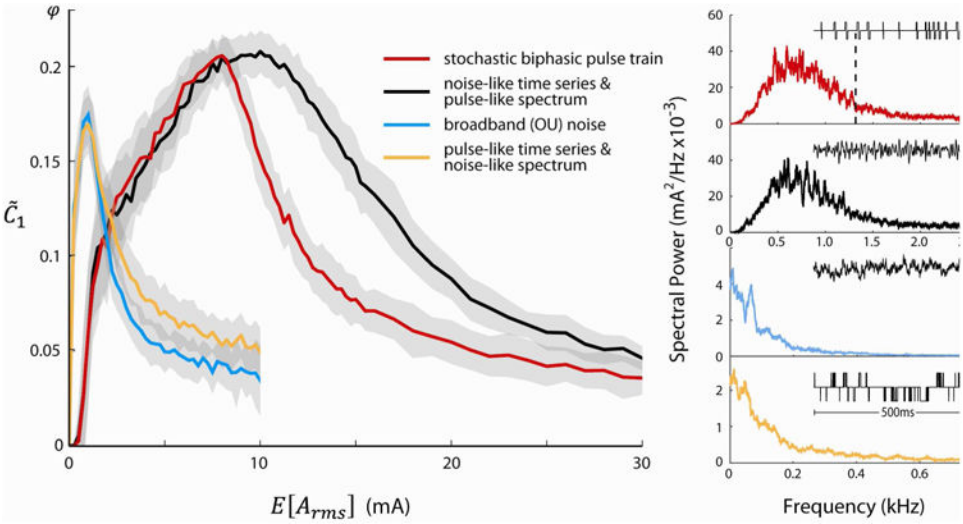

Fig. 7.

Responses of the model neuron to matched perturbation (noise) types indicate that the spectrum, rather than time domain structure, is responsible for the $\tilde{C}_1$ characteristics. Simulations were run for four perturbation types: basic broadband noise (blue, also see Fig. 5, blue traces), the stochastic biphasic pulse train (red), broadband noise-like time domain fluctuations with a spectrum matching that of the stochastic biphasic pulse train (black) and a train of stochastic square pulses with a spectrum matching the broadband noise (orange). Each trace is the mean of n=50 simulations and the gray bands are one standard deviation. Next to each spectrum is an inset of 500 ms of the corresponding time series, and the vertical axes of the times series are not to scale. The spectra axes are scaled differently because they are each calculated using the time series corresponding to their peak $\tilde{C}_1$ RMS amplitude, 9 mA RMS for the top two and 1 mA RMS for the bottom two. The stochastic biphasic pulse train (red) $\tilde{C}_1$ curve was generated by fixing the parameters at the value found in the middle white open circle in Fig. 3B and varying RMS amplitude, and the vertical dashed line marks the spectral lobe cutoff frequency. The broadband noise had r_c=0.5 ms^{-1}.

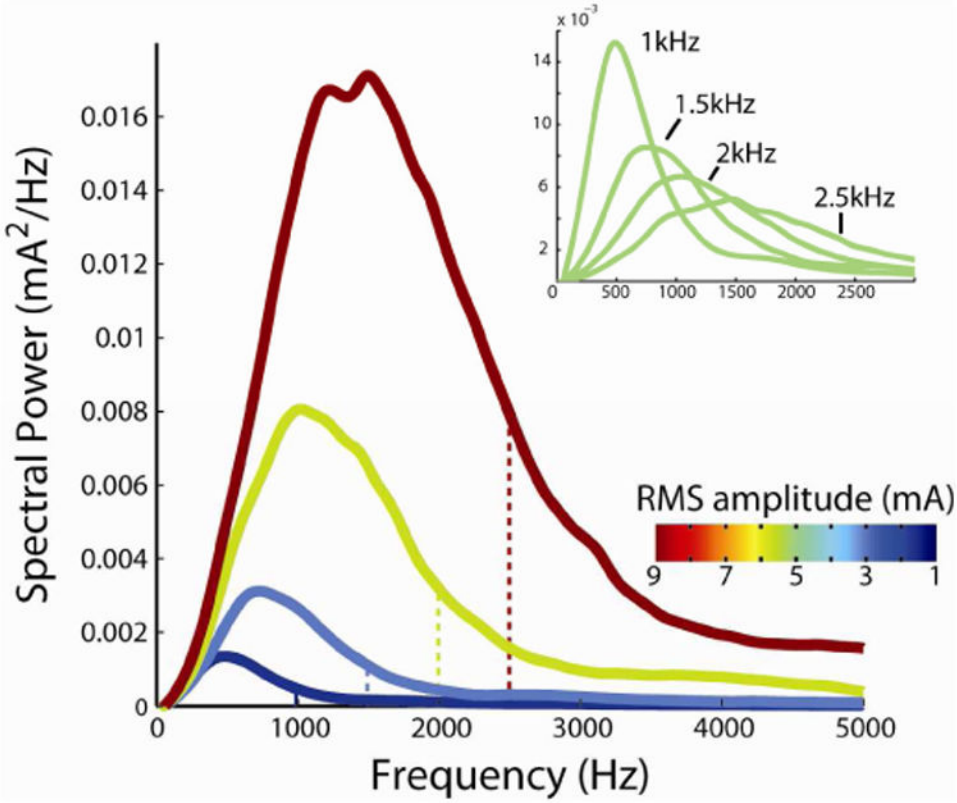

Fig. 8.

Strength of SR declines as high frequency spectral power increases. Each spectrum corresponds to a stochastic biphasic pulse train delivered during a simulation that, in combination with the input signal, yielded an average $\tilde{C_1}$ of 0.16. The spectra are colored by RMS perturbation amplitude, and their cutoff frequencies are indicated by dashed lines. The inset shows spectra of stochastic biphasic pulse trains with the same cutoffs as those in the main panel, but with equal RMS amplitudes (5 mA) and varied resulting $\tilde{C_1}$. For clarity, the curves plotted are interpolated spline fits of the power spectra.

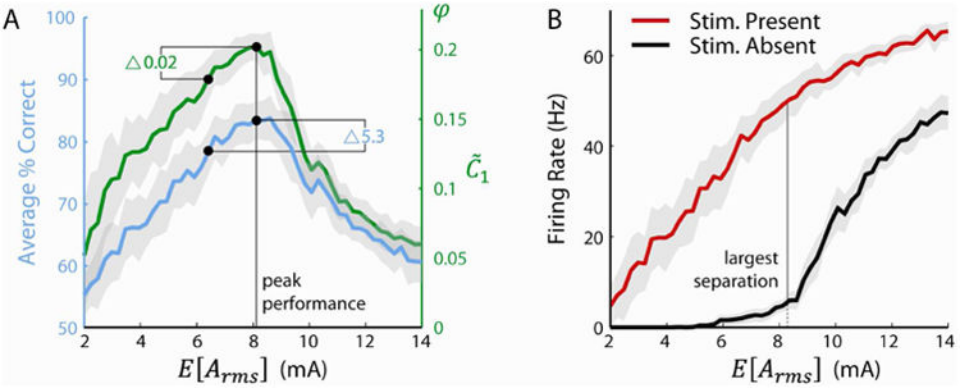

Fig. 9.

A model of the relationship between $\tilde{C}_1$ and performance in a sensory discrimination task. (A) A sub-threshold 6.5 mA input signal (described in Fig. 1) and stochastic biphasic pulse train perturbations were applied to the neuron model and the resulting $\tilde{C}_1$ is plotted (green), where the solid line is the average and the shaded region is one standard deviation. The perturbations were generated following the trajectory in parameter space denoted by the white line in Fig. 3B, example trials of which are given in Fig. 2A. The input signal was divided into bins where a crest of the input signal was either present or absent, and the average firing rate determined the neuron's classification of each bin as either having or not having an event. The average percentage correct classifications for each 2075 ms simulation were then calculated, and averaged over n=20 simulations for each point on the curve (blue). A reduction of 0.02 $\tilde{C}_1$ from peak $\tilde{C}_1$ results in a 5.3% loss in classification accuracy. (B) For each simulation the average firing rate during bins with (red) and without (black) events are plotted. Peaks in performance and $\tilde{C}_1$ curves correspond to the largest separation between the two firing rate curves (44.9Hz).

Table 1

Neuron model parameters.

Parameter Name	Symbol	Value
Sodium reversal potential	E_{Na}	115 mV
Max. sodium conductance	g_{Na}	120 mS
Potassium reversal potential	E_K	-12 mV
Max. potassium conductance	g_K	36 mS
Leakage reversal potential	E_L	10.6 mV
Max. leakage conductance	g_L	0.3 mS
Membrane capacitance	C_m	1 μF